AD 273 718

NAVWEPS REPORT 7812
NOTS TP 2811
COPY 234

ANALYTICAL VERSIONS OF PENETRATION PROCESSES

by

Werner Goldsmith
Research Department

ABSTRACT. In the interest of obtaining a comprehensive view of the penetration of bodies into solid plates some of the more prominent theoretical relations used to describe penetration processes are outlined and correlated. The velocity ranges to which these relations apply and the assumptions used in the analytical developments are summarized. Elastic behavior processes in impact are first discussed in order to establish lower bounds on the impact velocity for the formation of a crater. Various analytical representations of crater formation processes are summarized and the advantages of the theory of constant dynamic flow pressure are demonstrated by calculated results which agree well with experimental penetration data from several sources. The hydrodynamic theory of penetration and Öpik's theory of penetration are discussed in relation to these conclusions on crater formation.

U.S. NAVAL ORDNANCE TEST STATION

China Lake, California

February 1962

U. S. NAVAL ORDNANCE TEST STATION

AN ACTIVITY OF THE BUREAU OF NAVAL WEAPONS

C. BLENMAN, JR., CAPT., USN
Commander

WM. B. MCLEAN, PH.D.
Technical Director

FOREWORD

The material in this report represents part of a continuing applied research program in support of explosive ordnance problems at the U. S. Naval Ordnance Test Station. These studies were performed on an intermittent basis during the period July 1960 - September 1961, and were supported by funds under Bureau of Naval Weapons Task Assignments RMMO-42-107/216-1/F009-08-002 and RMMO-42-004/216-1/F008-08-006.

This report was reviewed for technical accuracy by Dr. Harry Kolsky, Brown University, and Mr. William A. Allen, U. S. Naval Ordnance Test Station.

CHAS. E. WARING
Head, Research Department

Released under
the authority of:
WM. B. McLEAN
Technical Director

NOTS Technical Publication 2811
NAVWEPS Report 7812

Published by ..... Research Department
Collation ..... Cover, 17 leaves, abstract cards
First printing ..... 315 numbered copies
Security classification ..... UNCLASSIFIED

1 Arthur D. Little, Inc., Cambridge (W. H. Varley)
2 Autonetics, A Division of North American Aviation, Inc., Downey, Calif.
Department 93, F. H. Gardner (1)
Technical Library, 393-53 (1)
2 Bell Aircraft Corporation, Buffalo (Technical Library)
1 Boeing Airplane Company, Seattle (Branch 7 Library)
2 Convair, San Diego (Engineering Library)
1 Douglas Aircraft Company, Inc., Long Beach
1 General Electric Company, Schenectady (LMEE Department, Librarian)
2 Grumman Aircraft Engineering Corporation, Bethpage, N. Y. (Library Director)
1 Jet Propulsion Laboratory, CIT, Pasadena (Dr. W. H. Pickering)
2 Lockheed Aircraft Corporation, Burbank, Calif.
1 Los Alamos Scientific Laboratory (Reports Librarian)
1 McDonnell Aircraft Corporation, St. Louis (Department 644, Engineering Library)
1 Midwest Research Institute, Kansas City (Librarian)
1 Norden Division, United Aircraft Corporation, Norwalk, Conn. (Library)
2 Northrop Corporation, Norair Division, Hawthorne, Calif. (Library)
1 Philco Corporation, Philadelphia, via RInsMat
1 Princeton University, Forrestal Research Center, Princeton, N. J. (Librarian)
2 Rohm and Haas Company, Redstone Arsenal Research Division (Librarian)
2 Solid Propellant Information Agency, Applied Physics Laboratory, JHU, Silver Spring
1 Southwest Research Institute, Department of Chemistry and Chemical Engineering, San Antonio (Dr. H. C. McKee)
1 Stanford Research Institute, Poulter Laboratories Menlo Park, Calif.
1 The Martin Company, Baltimore (I. E. Tuhy)
1 The Rand Corporation, Santa Monica, Calif. (Librarian)
1 The University of Chicago, Laboratories for Applied Sciences, Chicago (Library)
1 Thiokol Chemical Corporation, Reaction Motors Division, Denville, N. J. (Librarian)
1 Thiokol Chemical Corporation, Redstone Division, Redstone Arsenal
1 University of California, Berkeley (Werner Goldsmith)
1 University of Chicago, Institute for Air Weapons Research, Chicago (Library)
1 University of Denver, Denver Research Institute, Denver
1 Westinghouse Electric Corporation, Baltimore (Engineering Librarian)
13 Guided Missile Technical Information Distribution List No. 23, MML 200/23, dated 3 April 1961, Parts A and DW

INTRODUCTION

The process of penetration of particles or bodies, solid or liquid, into solid plates of large extent is extremely complicated and is, generally speaking, still relatively little understood. A rational description of the phenomena encountered is thus difficult, particularly in view of the fact that some of the experimental evidence obtained from virtually identical tests of different investigators leads to widely divergent results. Furthermore, it has been clearly demonstrated that different phenomena occur for different ranges of initial impact velocities and that different mechanisms of energy conversion play a dominant role in these various domains. Consequently, it cannot be expected that a single comprehensive theory can be readily evolved which will predict the penetration process in its totality for all materials, impact velocities, and collision geometries. Rather, most investigators have concentrated on developing theoretical relations, some rational, many empirical, deduced from available data and dimensional analysis, which are presumed to apply only within definite limits of the initial velocity.

It is the purpose of the present report to indicate some of the more prominent theoretical relations determined in this manner and to correlate this information. An indication will also be given of the nature and limits of the velocity ranges mentioned above and to discuss the various assumptions inherent in the analytical development. Some simple derivations are also included which purport to apply to the normal impact of spheres and cylinders on flat plates in a relatively low impact velocity regime.

ENERGY PROCESSES FOR PENETRATION

The energy processes encountered in penetration over the entire spectrum of impact velocities consist of the following types:

1. Energy of elastic wave propagation, E_e, resulting in elastic (recoverable) deformations of striker and target.

2. Energy of plastic wave propagation or plastic flow, E_p, resulting in permanent deformation of striker and target.

3. Energy of comminution or fragmentation of the colliding bodies, E_s.

4. Energy of bulk compression of the solids, W.

5. Shock heating energy due to the difference between adiabatic and shock compression of the solids, H.

6. Energy of vaporization and fusion of striker and target material, E_v.

7. Energy of polymorphic transitions and phase changes of the materials, E_t.

An energy balance for the penetration process can now be obtained by equating items 1 - 7 to ΔT, which represents the difference between the initial and terminal bulk kinetic energy of the projectile-target system. In addition, two other equations are derived from the laws of conservation of mass and momentum of the system. Provided sufficient information is available concerning the mechanical, physical, and thermodynamic behavior of the solids involved, these equations suffice, at least in theory, for a complete description of the behavior of the system.

In actual practice, however, severe difficulties are encountered in the solution of these equations. In fact, it is virtually impossible to predict damage parameters such as crater depths from these equations alone, and consequently recourse is almost universally taken to the use of models for this type of prediction. Furthermore, it is customary to delete terms in ranges where the contribution from the respective mechanism is expected to be very small relative to other terms. This is illustrated in the sequel where various domains of the penetration process are discussed in greater detail.

ELASTIC COLLISIONS

The process of elastic collisions does not, by definition, involve any permanent deformations in the colliding solids and as such would not appear to be of basic interest for the theoretical analysis of crater formation. The process is important, however, for the establishment of a lower bound of impact velocities for the generation of permanent craters which can then serve as a criterion for the presence or absence of such deformations. In the elastic regime, two distinct cases arise which are treated somewhat differently on a theoretical basis: (1) the elastic collision of two bodies with plane-ended surfaces in a direction normal to these surfaces, and (2) the elastic collision of two bodies with curved surfaces at the point of impingement. Both cases are well-known (Ref. 1 and 2) and only the most important results will be cited here.

Normal Collision of Two Plane-ended Bodies

Consider the collision of two uniform plane-ended rods of density ρ_1 and ρ_2, cross-sectional area A_1 and A_2, and rod wave velocity c_1 and c_2, respectively, with a relative impact velocity v_o, as shown in Fig. 1.

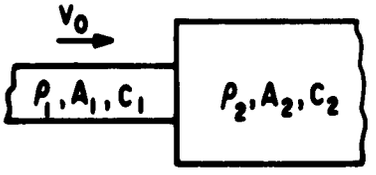

FIG. 1. Normal Collision of Two Plane-ended Bodies.

The rod wave velocity c is defined here as

$$c = \sqrt{\frac{E}{\rho}} \tag{1}$$

where E is the modulus of elasticity, and represents the rate of propagation of a plane wave in a relatively narrow rod. At the instant of impact, two elastic waves are generated in both bars, whose amplitudes may be determined from the well-known equation

$$\sigma = \rho c v \tag{2}$$

and the condition of equality of forces and particle velocities v at the contact surface, given by

$$\sigma_1 A_1 = \sigma_2 A_2 \qquad v_o - v_1 = v_2 \tag{3}$$

as

$$\sigma_1 = \frac{v_o A_2}{\left[\frac{A_2}{\rho_1 c_1} + \frac{A_1}{\rho_2 c_2}\right]} \qquad \sigma_2 = \frac{v_o A_1}{\left[\frac{A_2}{\rho_1 c_1} + \frac{A_1}{\rho_2 c_2}\right]} \tag{4}$$

The particle velocities induced in the bodies are given by

$$v_1 = \frac{v_o \rho_2 c_2 A_2}{A_1 \rho_1 c_1 + A_2 \rho_2 c_2} \qquad v_2 = \frac{v_o \rho_1 c_1 A_1}{A_1 \rho_1 c_1 + A_2 \rho_2 c_2} \tag{5}$$

For normal contact, the wave in the smaller rod is completely plane; the wave in the larger rod is initially spherically divergent, but will rapidly approach the character of a plane wave, with an amplitude given by Eq. 4, provided the ratio of areas of the rods is not too great. If one of the colliding bodies approaches the dimensions of a semi-infinite target ($A_2/A_1 \gg 1$), the wave in this body will be essentially spherically divergent throughout and will travel with dilatational velocity $\bar{c}_2 = \sqrt{(\lambda + 2G)/\rho}$ where λ and G are the Lamé constants. The amplitude at any distance r from the contact point for this spherical wave is approximated by

$$\sigma_2 = \frac{1}{r} \frac{\rho_1 c_1 \rho_2 \bar{c}_2 v_o}{\rho_1 c_1 + \rho_2 \bar{c}_2} \tag{6}$$

If body 2 can be regarded as completely rigid ($E_2 = \infty$), the stress produced in bar 1 can be determined from Eq. 4 with $c_2 = \infty$, or from Eq. 2 with v replaced by v_o; this situation yields the maximum stress in bar 1 for this type of impact. The stress at the contact surface is maintained until relieved by a reflected wave emanating from a free end of either bar.

The threshhold of plastic deformation is attained when the stress produced by the collision, given by Eq. 4, reaches the dynamic compressive yield stress of the material. This quantity is usually in excess of the corresponding static value by various amounts; for mildly strain-hardening materials without a definite yield point such as aluminum and some alloy steels, the excess is from about 15 to 25%. For example, 2024-T4 aluminum alloy, which has a static yield stress of about 53,000 psi, would have a dynamic yield stress of about 65,000 psi. On the other hand, for materials with a definite yield point, such as mild steel, the excess may be from 100 to 200%. Specific literature references for the material under consideration should be consulted for the determination of the dynamic compressive yield stress (Ref. 3-5).

Collision of Bodies With Rounded Contact Surfaces

The impingement of two bodies, whose contact surfaces can be represented analytically by equations of the second degree, has been invariably analyzed by means of the Hertz law of contact. This relation was originally developed on the basis of an electrostatic analogy to specify the compression of two elastic bodies in contact under static loading conditions, but was also used by its originator and numerous subsequent investigators for a description of collision processes involving such bodies (Ref. 1, 6, 7). The excellent agreement observed between the results of numerous impact experiments and the predictions of the Hertz theory has provided confidence in the postulate that the Hertz law applies also under dynamic conditions provided the elastic limit of the material is not transcended. Strangely enough, it was also found that the Hertz law appears to predict approximately a number of collision parameters, such as the duration of contact and the maximum force of the collision

even when permanent craters are produced -- a condition which is in contradiction with the basic postulate of the theory. However, the elastic analysis can not, of course, predict the dimensions of such a permanent indentation since it presumes completely elastic restitution.

Briefly, the force of compression F between the bodies is given by the relation (Ref. 1)

$$F = k_2 \alpha^{3/2} \tag{7}$$

where α is called the approach between the bodies, defined as the difference in the distance between two points, one in each body, located along the common normal at the initial point of contact and sufficiently far removed from the contact region as to be in an essentially unstrained domain at all times, at the initial instant of contact and at any subsequent instant while the bodies are still compressed. The quantity k_2 depends upon the elastic constants of the bodies and is, furthermore, in general a complicated integral function of the geometry of the surfaces in contact. The contact area is an ellipse of semi-axes a and b, and the pressure distribution p across this ellipse is given by

$$p = \frac{3F}{2\pi ab} \sqrt{1 - \frac{x^2}{a^2} - \frac{y^2}{b^2}}, \quad x \leq a, \; y \leq b \tag{8}$$

relative to axes x and y extending along the semi-major and semi-minor axes a and b, respectively. Terms a and b can also be evaluated by means of integral relations from the elastic and geometrical properties of the bodies. Contact is terminated whenever the approach α returns to zero.

For the particular case when the two bodies (distinguished here by subscripts 1 and 2) are spheres of radius R_1 and R_2, respectively, or for the case of a sphere and a plane surface ($R_2 = \infty$), the value of k_2 assumes a particularly simple form. In this event, with $\Theta \equiv (1 - \mu^2)/\pi E$, where μ is Poisson's ratio

$$k_2 = \frac{4}{3\pi(\Theta_1 + \Theta_2)} \left[\frac{R_1 R_2}{R_1 + R_2}\right]^{1/2} \qquad \text{for two spheres}$$

$$k_2 = \frac{4}{3\pi(\Theta_1 + \Theta_2)} \sqrt{R_1} \qquad \text{for a sphere and a plane surface} \tag{9}$$

The contact area is a circle of radius a, related to the approach by the equations

$$a^2 = \frac{\alpha R_1 R_2}{R_1 + R_2} \qquad \text{for two spheres}$$

$$a^2 = \alpha R_1 \qquad \text{for a sphere and a plane surface} \tag{10}$$

respectively, and the pressure distribution, Eq. 8, may be written as

$$p = \frac{3F}{2\pi a^2}\sqrt{1 - \frac{r^2}{a^2}}, \quad r \leq a \tag{11}$$

where r is the radial coordinate.

The collision of two such bodies can now be written in terms of the equation of motion,

$$\frac{m_1 m_2}{m_1 + m_2}\ddot{\alpha} = -F \tag{12}$$

and substitution of Eq. 7 then yields the relation

$$\ddot{\alpha} = -k_1 k_2 \alpha^{3/2} \tag{13}$$

where $k_1 \equiv (m_1 + m_2)/m_1 m_2$. If body 2 can be regarded as semi-infinite ($m_2/m_1 \gg 1$), the quantity k_1 may be written simply as $k_1 = 1/m_1$. Integration of Eq. 13 yields

$$\frac{1}{2}(\dot{\alpha}^2 - v_o^2) = -\frac{2}{5} k_1 k_2 \alpha^{5/2} \tag{14}$$

where v_o is the initial impact velocity, and since $\dot{\alpha} = 0$ at the maximum approach α_m, this term can be evaluated from the expression

$$\alpha_m = \left[\frac{5v_o^2}{4k_1 k_2}\right]^{2/5} \tag{15}$$

The average pressure across the contact circle at the instant of maximum approach is

$$p_{av}\frac{F_{max}}{\pi a_{max}^2} = \left[\frac{5v_o^2}{4k_1}\right]^{1/5} k_2^{4/5}\frac{(R_1 + R_2)}{\pi R_1 R_2} \tag{16}$$

and the maximum pressure at this instant, p_{max}, may be determined from Eq. 11 as

$$p_{max} = \frac{3}{2} p_{av} = \frac{3}{2}\frac{F_{max}}{\pi a_{max}^2} \tag{17}$$

located at the center of the circle. The total duration of contact may be evaluated as

$$t = 2\int_0^{\alpha_{max}} \frac{d\alpha}{\dot{\alpha}} = 2\int_0^{\alpha_{max}} \frac{d\alpha}{\sqrt{v_o^2 - \frac{4}{5} k_1 k_2 \alpha^{5/2}}} = 2\frac{\alpha_{max}}{v_o}\int_0^1 \frac{dZ}{\sqrt{1 - Z^{5/2}}} =$$

$$\frac{4}{5}\sqrt{\pi}\,\frac{\alpha_{max}}{v_o}\,\frac{\Gamma(\frac{2}{5})}{\Gamma(\frac{9}{10})} = 2.9432\,\frac{\alpha_{max}}{v_o} \qquad (18)$$

Davies (Ref. 7) computed the stress distribution in a semi-infinite elastic solid when loaded by a steel sphere (Fig. 2), and from this stress field determined the values of the principal stresses (stresses acting on an infinitesimal cubic element of the solid, so oriented that no shear stresses act on the faces of the cube) throughout the body. This calculation is necessary if the state of incipient plastic yielding of the semi-infinite body is to be ascertained, since all criteria for this condition, postulated thus far for multi-axial stress conditions, involve the magnitudes of the principal stresses. The two most commonly used criteria, which meet the experimentally observed condition that hydrostatic pressure has little, if any influence on yielding, are the so-called Tresca and von Mises conditions, given, respectively, by (Ref. 8)

$$\sigma_1 - \sigma_3 = \text{constant} \qquad (19)$$

$$(\sigma_1 - \sigma_2)^2 + (\sigma_1 - \sigma_3)^2 + (\sigma_2 - \sigma_3)^2 = \text{constant} \qquad (20)$$

where σ_1 and σ_3 are the maximum and minimum (algebraic) principal stresses. The constant in Eq. 19 is usually chosen as σ_Y, the yield stress is simple tension or compression (which are assumed to be equal for most metals), while the constant in Eq. 20 is chosen as $2\sigma_Y^2$. The two criteria differ to some extent in the prediction of the maximum shear stress τ_{max} for various stress combinations, i.e., $\tau_{max} = 1/2\ \sigma_Y$ for Eq. 19 and $\tau_{max} = 2\sigma_Y/\sqrt{3}$ for Eq. 20, but as indicated by these values, the differences are not too great. Equation 20 has been found to predict more accurately the yield condition for most ductile metals, but Eq. 19 is simpler to use and has thus found considerable favor in analytical investigations.

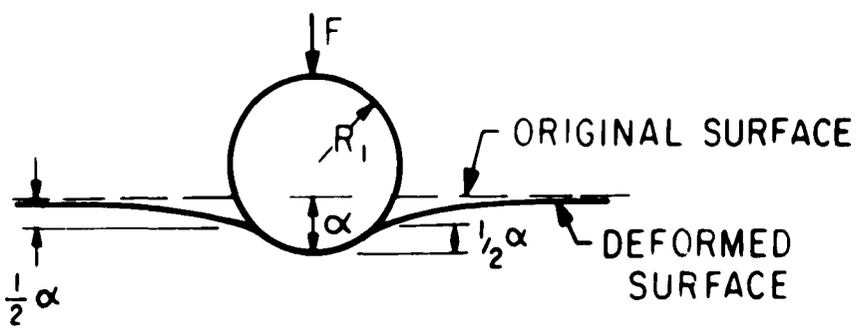

FIG. 2. Stress Distribution in a Semi-infinite Elastic Solid When Loaded By a Steel Sphere.

The analysis performed by Davies utilized Eq. 19 for the prediction of an incipient state of yielding. By suitable combination of the principal stresses in the semi-infinite body, he determined that the maximum difference of the principal stresses in such a body exhibiting a Poisson's ratio of 0.286 (corresponding to steel) could be expressed by

$$\sigma_1 - \sigma_3 = 0.63\ p_{max} \tag{21}$$

where p_{max} is given by Eq. 17. When Eq. 21 is then equated to the dynamic yield stress in simple tension or compression, it is possible to determine either the minimum impact velocity required to produce plastic deformation for a material with a known value of the dynamic yield stress in tension or compression, or else to experimentally determine such a limiting stress by observing the first noticeable deformation of an optically flat surface subjected to the impact of a sphere dropped from successively greater heights. In either case, the equation for this case may be determined from Eq. 21 and 16, with $m_2/m_1 = R_2 = \infty$, as

$$\sigma_{Y_{Dynamic}} = 0.63\ p_{max} = 0.63 \times \frac{3}{2\pi R_1} \left[\frac{5}{4} v_o^2 m_1\right]^{\frac{1}{5}} \left[\frac{R_1}{3\pi(\theta_1 + \theta_2)}\right]^{\frac{4}{5}} \tag{22}$$

It should also be noted that the position of the maximum difference of the principal stresses does not fall on the circle of contact, but rather a certain distance vertically below the center of this circle, so that plastic flow is initiated in the interior of the body. For the case examined by Davies (Ref. 7), corresponding to steel, this distance is 0.48a where "a" is the radius of the circle of contact.

Davies observed that hard steel spheres with diameters of the order of 0.25 inch produce permanent indentations in armor plate (static yield stress, 155,000 psi; ultimate tensile strength, 343,000 psi; Brinell hardness number 321) when dropped from as low a height as 0.35 cm. This impact corresponds to an initial impact velocity of $v_o = 10.35$ in/sec = 0.861 ft/sec, an extremely small velocity, yet produced a maximum stress $p_{max} = 289{,}000$ psi at the center of the contact circle, corresponding, from Eq. 21, to a dynamic yield stress of 182,000 psi. It can be concluded from this sequence of observations that if permanent indentations can be produced by solid spheres in a material as hard as armor plate at these minimal velocities, that purely elastic impacts by spheres against plane surfaces virtually do not exist in practice and, furthermore, that the elastic range can normally be completely neglected under actual impact conditions of this type. This contrasts sharply with the situation encountered in the impact of plane surface, where permanent indentations are not expected to occur until the stresses σ_1 or σ_2 given by Eq. 4

attain the dynamic compressive yield stress of the material, which requires substantially larger impact velocities than for the case of a sphere against a plane surface.

TECHNIQUES OF ANALYSIS FOR THE FORMATION OF PERMANENT CRATERS

The two principal approaches for the analysis of the formation of permanent craters can be described on the following basis: (1) techniques employing the theory of plasticity, usually applied to an ideally plastic solid (i.e., a solid in which the yield stress under uni-axial load remains constant with increased deformation; this contrasts to a work-hardening solid in which this stress increases with further deformation), and (2), a description of the behavior of the materials by means of the continuity equations (Bernoulli equations) for a perfect fluid, compressible or incompressible, with particular reference to the penetration of targets by jets. It should be noted that the theory of plasticity always postulates complete incompressibility of the materials. Some other theories of penetration utilizing the concept of incompressible fluid flow, such as advanced by Öpik (Ref. 9 and 10), are closely related to the analysis based on plasticity arguments.

The theory of plasticity has, in general, been developed only for equilibrium processes and must thus be adapted to dynamic conditions in order to permit application to the process of crater formation. Even for static loading, however, relatively few deformation problems have been solved in a completely rigorous fashion in the plastic regime. While, for example, the case of indentation of a semi-infinite solid with a plane surface by a flat die of infinite length, loaded by a uniform normal pressure (two-dimensional case), has been analyzed exactly by means of the plasticity criterion given by Eq. 19 or 20, (Ref. 8), the corresponding three-dimensional problem of the penetration of flat circular punch into such a solid has been evaluated only approximately due to the necessity of using a plasticity criterion having no physical basis (Ref. 11). The latter, known as the Haar-Karman criterion, permits an integration of the stress field, which the criteria expressed by Eq. 19 or 20 will not permit, but requires that the two smaller principal stresses, σ_2 or σ_3 are equal and then utilizes Eq. 19. The indentation of a sphere into a semi-infinite solid, which is also a three-dimensional problem, has likewise only been solved by means of the Haar-Karman criterion. Consequently, the available solutions of three-dimensional problems of plastic indentations, while probably reasonably accurate on the whole, must still be regarded as approximations in view of the enforced equality of two of the principal stresses, a condition which actually will not prevail.

The actual solutions of all these plastic indentation problems, regardless of the plasticity criterion employed, has been carried out by the

method of slip-lines. It is assumed here that plastic flow occurs whenever the maximum shear stress reaches a critical value k (where $k = 1/2\ \sigma_Y$ according to Eq. 19 and $k = 0.575\ \sigma_Y$ according to Eq. 20) and that the effects of elastic strains can be neglected. The flow of the material can then be determined by integrating along these slip-lines which are defined as the families of curves whose directions at every coordinate in the body correspond to those of the maximum shear strain rate. The details of this procedure are quite involved and will not be cited here, but a full exposition of such techniques is given in Ref. 11, pp. 134 ff.

In the application of the theory of plasticity to cratering problems, it is, of course, necessary to employ the value of the dynamic yield stress rather than the corresponding static value in the analysis. Furthermore, it is necessary to account for the inertia of the target material in the appropriate kinetic relations; this quantity is usually neglected in slip-line solutions since the resistive forces of the target normally far exceed inertial terms in static deformation problems. For impact conditions, however, the magnitude of this term is frequently not negligible. It will be assumed in the development of the theory based upon plasticity arguments, that fragmentation, vaporization, and shock heating of the colliding objects is absent.

From the available slip-line solution, it has been possible to determine the pressure under the indenter which must be overcome to produce plastic indentation. This pressure is greater than the yield point stress of the substance, since the portion of the semi-infinite target immediately below the indenter is confined by surrounding material which must be brought to a state of incipient plastic flow before actual penetration can take place. This is due to the fact that actual changes in configuration of the target must be initiated at a free surface. The values of the pressure so computed and other pertinent information will now be given for the known slip-line solutions (Ref. 8 and 11).

It will first be assumed that no friction exists between indenter and target. Then, for the two-dimensional case of a flat die cited above, the pressure produced is uniform across the die and of amount $p = 2k(1 + \pi/2)$. Thus, according to the Tresca yield condition, $p = 2.571\ \sigma_Y$ and according to the Mises condition, $p = 2.96\ \sigma_Y$. The slip lines consist of arcs of circles and straight lines making 45-degree angles with the free surfaces and the interface, and flow at the interface occurs along these lines with a velocity $(\sqrt{2})\dot{x}$ where $\dot{x}$ is the velocity of the die. This solution is exact.

For the circular punch and the ball indentation problem, the solution is only approximate due to the restrictions of the Haar-Karman plasticity criterion. Even for the frictionless case, however, the pressure distribution across the interface is not uniform; the nature of the variation is shown in Fig. 3. However, the mean value of the pressure, $p_m = 2.84\ \sigma_Y$ for a circular punch and $p_m = 2.66\ \sigma_Y$ for a sphere (Ref. 11), do not differ significantly from the corresponding value for the die. In neither

case are the slip lines uniform straight lines; however, for the punch, the intersection of the slip lines with the interface still occurs at 45 degrees, and thus the velocity of the material below the indenter is still given by $(\sqrt{2})\dot{x}$. On the other hand, for the ball, this angle varies from about 45 to 20 degrees, and thus the velocity of the material below the striker will range from $(\sqrt{2})\dot{x}$ to $2.75\dot{x}$, with a mean value of about $2\dot{x}$.

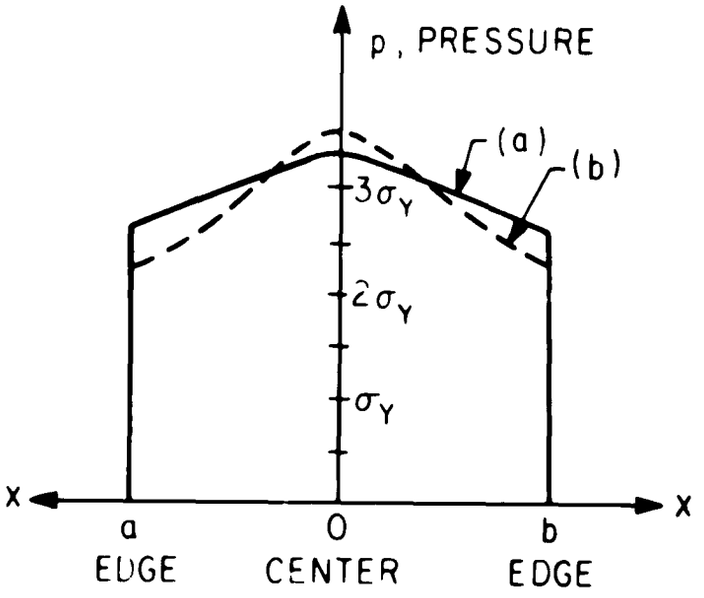

FIG. 3. Pressure Distribution According to the Haar-Karman Criterion and Slip-line Solutions for (a) a Flat Circular Punch (b) a Rigid Sphere Indenting a Semi-infinite Target (Ref. 11).

The effect of friction is to further distort the uniformity of the pressure distribution across the face of the indenter, and furthermore, to increase the effective mean pressure required to produce plastic indentation. While a quantitative evaluation of this effect is difficult, it has been demonstrated for a case comparable to those described above, that the increase in pressure is about $(1 + f)$, where f is the coefficient of friction. This condition applies, however, only as long as $fp < k$ where $k = \tau_Y$ is the yield stress in shear; this amounts to a maximum value of the coefficient of friction f of about 1/6, a very low value for the contact of metal surfaces. For higher values of the coefficient of friction, slip will occur within the skin of the metal below the indenter rather than at the interface, and the pressure resisting indentation may be considerably in excess of $1.5\ p_m$, where p_m is the flow pressure opposing penetration under frictionless conditions (Ref. 11).

The above considerations have been presented in order to examine whether or not the concept of a constant flow pressure could be satisfactorily employed for the analysis of penetration problems based on a theory of plasticity and, if so, how this flow pressure could be adduced from some other known or readily determinable mechanical property of the material. It should be mentioned that the mean flow pressure determined analytically for the penetration of a sphere on the basis of the approximate Haar-Karman criterion was somewhat dependent on the depth of penetration, decreasing slightly with increasing depth under static loading conditions (Ref. 11). Experiments under these circumstances, indicate, however, that a slight increase of this parameter with depth of indentation occurs (Ref. 11). Other tests under dynamic conditions involving the impact of a sphere on a plane surface at relatively low initial velocities have been reported (Ref. 12) which indicate a virtually constant value for the flow pressure. On the other hand, similar experiments at higher initial velocities indicated a variation of the magnitude of the flow pressure during the course of the penetration process (Ref. 13). It is not unlikely that the flow pressure may vary with strain -- or loading-rate. It should also be borne in mind that the analysis of the static indentation process was carried out for an ideally plastic material, which actually does not exist, and that the effect of elastic strains was neglected. Nevertheless, on balance, it appears as though the assumption of a constant flow pressure does not violate too seriously the actual deformation pattern of the material. Furthermore, this type of postulate permits a drastic simplification of an otherwise almost intractable problem and might even be rationalized on the basis of the current relative ignorance concerning the actual material properties under impact conditions, which might lead to greater errors than basically inherent in this assumption. A calculated value for this pressure based on a known dynamic yield stress can be obtained with reasonable accuracy only if existing friction is virtually eliminated; in this case, the magnitude of the pressure is approximately given by $p_m \approx 2.9\ \sigma_Y$. The presence of friction will, however, modify such a value significantly. This feature will be further illustrated in a subsequent section where the data from a number of experiments employing flat, cylindrical projectiles fired against a semi-infinite target at normal incidence are examined.

Any theory of penetration based solely on the concept of plasticity must necessarily fail when the impact velocity attains a sufficient magnitude to alter appreciably the density of either striker or target. This situation probably occurs long before either fusion or vaporization of the bodies takes place, so that the former condition can serve as a limit of applicability of the plasticity theory. It may be possible to set a predetermined bound, perhaps of the order of 1-2% on the compressibility of the substances, beyond which the use of a hydrodynamic model for the two bodies is indicated. However, it may be possible to use the theory of plasticity in the event of fragmentation of either striker or target with the aid of an appropriate energy balance provided the other effects, cited above, are not present to a significant degree.

Any success of the theory of plasticity in correctly predicting penetration phenomena is coupled to the ratio of the energy which is consumed in the plastic deformation of the target as opposed to the amount used in providing kinetic energy. In the regime of low velocity impacts, most of the energy of the striker is utilized in performing quasi-static work during the penetration process. As the velocity of the projectile is increased, a successively larger percentage of this energy is converted into kinetic energy of the target area and its environs, and a hydrodynamic analysis becomes more realistic.

The hydrodynamic theory of penetration has found its greatest use in the prediction of crater depths and volumes produced in targets by jets (Ref. 14-19). This type of analysis suffers from a number of defects on theoretical grounds alone. The most serious deficiency is the assumption of a steady state for the phenomenon, a condition which is surely not realized, particularly during the initial phase of the crater formation. This postulate is primarily responsible for the inapplicability of this theory to the penetration of targets by a single solid projectile, since such an event can hardly be regarded as an equilibrium process (unless, conceivably, perforation of a very thin target is considered where the change of velocity of the projectile is small). Furthermore, the steady-state hypothesis implies essentially an infinite reservoir of jet material, so that starting and stopping of the jet have no effect on the phenomenon. This requirement also implies the absence of a velocity gradient in the jet, although a correction for the existence of such a gradient has been proposed (Ref. 15). A recent innovation has also been an attempt to incorporate variations in jet density in the analysis.

In the elementary version of the hydrodynamic jet penetration process, both target and jet are assumed to be incompressible, which is an unnecessary postulate. While Cook (Ref. 17) has added a correction term accounting for the compressibility of the target, the compressibility of the jet is not taken into account and, furthermore, the inertial effects of the target are calculated on the basis of its original density. The effect of target strength in resisting penetration, while neglected in the original derivation on the basis of its order of magnitude relative to the inertial terms, has been subsequently incorporated in a number of derivations (Ref. 17-19). The existence of secondary penetration, i.e., a further increase in the depth of the crater after cessation of jetting, was also stipulated due to the necessity of reducing the inertial pressure, generated by the flow of the material, to the level of the dynamic yield strength of the material. This dissipation process was postulated to consist of radial flow by Pack and Evans (Ref. 18) whence the depth of the crater due to secondary penetration was simply taken as r, the radius of the hole produced by the jet. Cook (Ref. 17) incorporated the secondary penetration in the calculation of the crater volume by means of a force balance in which the secondary penetration process was governed by the same strength function as in primary penetration. The same author also suggested a method of accounting for shock heating and possible "impact explosions" (instantaneous vaporization of the materials). Some

details of the proposed relations covering these topics will be reproduced in a subsequent section.

Another version of the normal impact of an elastic, cylindrical projectile on a plastically deformable, semi-infinite target has been proposed by Backman (Ref. 20 and 21). Basically, the technique consists of an impedance matching of the two bodies at the interface, and from the requirements of equality of particle velocity and stress at this point deriving relations of the form given by Eq. 4 and 5 for the stress wave propagation into projectile and target. The return of the wave reflected at the free end of the cylinder to the impact point produces a new set of compatibility conditions at this station, which may be determined by superposition. It is assumed that the wave velocity in the projectile is that of the rod wave, c; the velocity in the target is the dilation wave $\bar{c}$, and wave reflection in the target is ignored. The impact velocity is restricted to a regime which does not produce fracture in the target.

The wave action is analyzed on the basis that, for the lower range of impact velocities, the reaction of the target is essentially elastic-plastic deformation occurring only on the crater sides. At higher velocities, the state of the target at the interface is plastic, giving rise to a proportionately lower penetration resistance than in the elastic realm. While the details of the analysis in the two references just cited differ somewhat, it is predicted that the functional relation between the depth of penetration and impact velocity consists essentially of two straight lines, such as sketched in Fig. 4, with empirically determined constants v_c and v_l selected to give the best fit of the data. (Note: in Ref. 20, a more complicated analysis attempting to account for work-hardening of the solid necessitates the selection of three empirically determined constants.) The abrupt transition from elastic to plastic resistance of the target occurs at an appreciable impact velocity, amounting to from 300 to 400 ft/sec for a 1/4-inch-diameter projectile of tool steel against a 1 1/4-inch-thick plate of 2024-T4 aluminum.

On the basis of the previous discussion, it does not appear reasonable that an elastic reaction should be expected at the interface even at low velocities, provided any cratering takes place at all. This is due to the fact that the initial regime of plastic flow has been shown to occur directly under the indenter, although not at the interface. While no flow of the material is expected until a band emanating from the initial zone of plastic deformation has reached a free surface, and while such a region of plastic deformation is confined by the surrounding, elastically strained material, it can not be accepted that the target just below the indenter should behave elastically in the domain of measurable craters, since slip-lines must always emanate from this domain (Ref. 8). It also appears unreasonable that there should be such an abrupt and distinct transition from elastic to plastic behavior of the target below the indenter. Rather, it would seem that it might be possible to neglect the elastic resistance of the target altogether (except for the determination of a minimum impact velocity producing measurable penetration) and

analyze the process on the basis of a constant flow pressure. It will be shown in the next section that such a procedure produces an excellent fit to all the data presented in Ref. 19 and 20, as well as of additional test results provided by Backman. Furthermore, this simple theory requires only a single experimental constant, the dynamic flow pressure, which can be checked against the value predicted from the theory of plasticity.

PENETRATION OF A RIGID INDENTER INTO A SEMI-INFINITE TARGET EXHIBITING A CONSTANT FLOW PRESSURE

It will be assumed for the purposes of the present analysis that the material behavior of a semi-infinite target resisting penetration can be described by means of the concept of a constant flow pressure. It is further stipulated that elastic deformations in the target can be neglected relative to permanent indentations; however, a threshhold of permanent deformation, depending upon the materials considered and the initial impact velocity, will exist, which can be described in terms of known mechanical properties of the solid. The striker will be considered to remain entirely elastic throughout the cratering process, and the energy contained in the waves travelling in the striker will be neglected.

First, consider the normal penetration of a rigid circular cylinder into a semi-infinite target in the absence of friction as shown in Fig. 5. The resistance to penetration will consist of the mean flow pressure, p_m, and the inertial resistance of flow of the target. The latter is given by $1/2\ \rho_t \dot{x}^2$, where ρ_t is the target density and x the coordinate in the direction of penetration, even though the slip-line flow has a velocity of $(\sqrt{2})\dot{x}$ at 45 degrees to the interface, since only the normal velocity component can exert a resistive force on the face of the indenter. The equation of motion is given by

$$-\frac{m\ddot{x}}{A} = \frac{1}{2}\rho_t \dot{x}^2 + p_m \quad \text{or} \quad \ddot{x} + \frac{A\rho_t \dot{x}^2}{2m} + \frac{Ap_m}{m} = 0 \tag{23}$$

where $m = AL\rho_p$ is the mass of the projectile, and A, L, and ρ_p its cross-sectional area, length, and density, respectively. With $v \equiv \dot{x}$, integration of Eq. 23 yields

$$t = \int_0^t dt = -\int_{v_o}^{v} \frac{2m}{\rho_t A} \frac{dv}{v^2 + \frac{2p_m}{\rho_t}} = -\frac{2m}{\rho_t A}\sqrt{\frac{\rho_t}{2p_m}} \tan^{-1} v\sqrt{\frac{\rho_t}{2p_m}}\Bigg|_{v_o}^{v}$$

$$= \frac{m}{A}\sqrt{\frac{2}{\rho_t p_m}}\left[\tan^{-1} v_o\sqrt{\frac{\rho_t}{2p_m}} - \tan^{-1} v\sqrt{\frac{\rho_t}{2p_m}}\right] \tag{24}$$

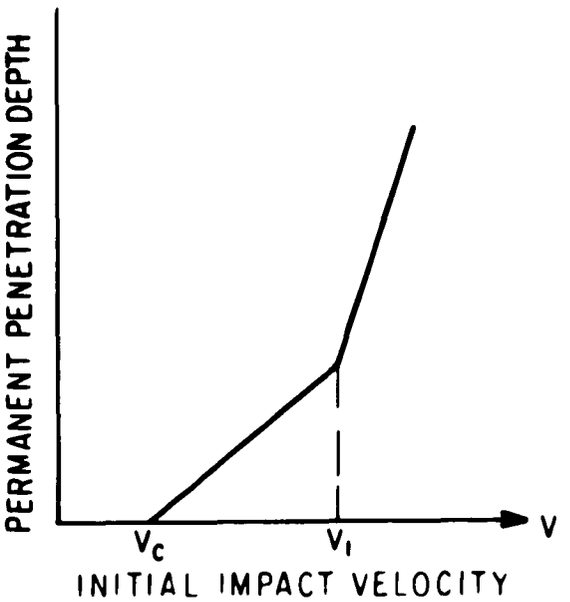

FIG. 4. Initial Impact Velocity vs. Penetration Depth.

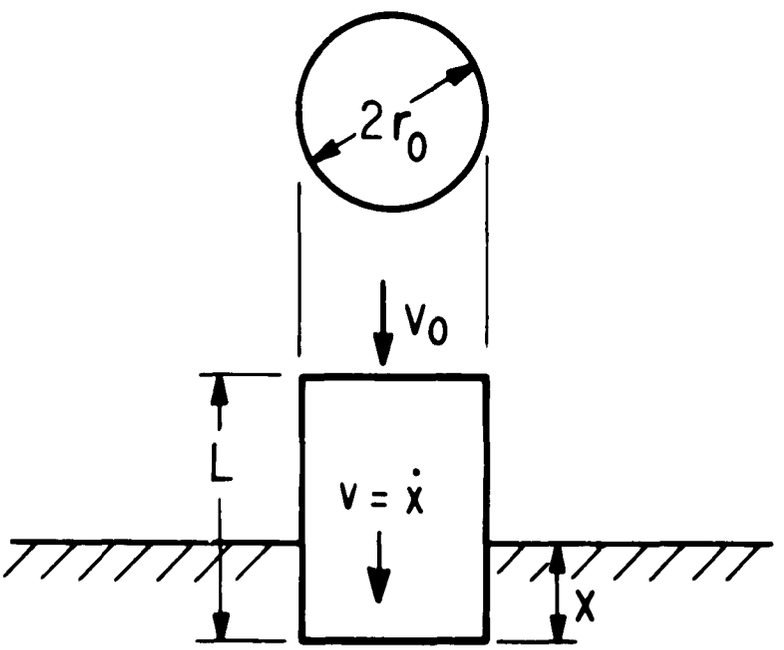

FIG. 5. Normal Penetration of a Rigid Circular Cylinder into a Semi-infinite Target in the Absence of Friction.

and

$$v = \frac{dx}{dt} = \sqrt{\frac{2p_m}{\rho_t}} \tan\left[\tan^{-1} v_o \sqrt{\frac{\rho_t}{2p_m}} - \frac{At}{m}\sqrt{\frac{p_m\rho_t}{2}}\right] \tag{25}$$

A second integration provides the result

$$x = \frac{m}{\rho_t A}\left\{\ln\left|\cos\left(\tan^{-1} v_o\sqrt{\frac{\rho_t}{2p_m}} - \frac{At}{m}\sqrt{\frac{\rho_t p_m}{2}}\right)\right| - \ln\left|\cos\left(\tan^{-1} v_o\sqrt{\frac{\rho_t}{2p_m}}\right)\right|\right\} \tag{26}$$

and the maximum penetration, x_{max}, occurring at time t_{max} when $v = 0$, where

$$t_{max} = \frac{m}{A}\sqrt{\frac{2}{\rho_t p_m}} \tan^{-1} v_o \sqrt{\frac{\rho_t}{2p_m}} \tag{27}$$

is then given by

$$x_{max} = \frac{m}{\rho_t A} \ln\sqrt{\frac{v_o^2\rho_t}{2p_m} + 1} = \frac{\rho_p L}{\rho_t} \ln\sqrt{\frac{v_o^2\rho_t}{2p_m} + 1} \tag{28}$$

Whenever $\frac{v_o^2\rho_t}{2p_m} \ll 1$, Eq. 28 can be expressed as

$$x_{max} \approx \frac{\rho_p L v_o^2}{2p_m} \quad \text{or} \quad \frac{x_{max}}{L} \approx \frac{\rho_p v_o^2}{2p_m} \tag{29}$$

which shows that the dimensionless penetration, x_{max}/L, varies as the square of the initial impact velocity. The same result can, of course, be obtained by neglecting the flow pressure term in Eq. 23 and writing the equation of motion as the energy balance

$$\frac{1}{2} m v_o^2 = p_m A x_{max} \tag{30}$$

It should be noted that the result obtained here is in direct contrast with the conclusions of Backman.

To account for the fact that a finite initial velocity v_o is required to produce any permanent deformation, the term v_o in Eq. 28 to 30 will be replaced by the quantity $v_o - v_c$. This critical velocity v_c can be computed from the elastic shock matching given by the modified form of Eq. 4 with σ_2 replaced by the yield stress σ_Y, yielding

$$v_c = \frac{\sigma_Y\left[\rho_t\bar{c}_t + \rho_p c_p\right]}{\rho_t\bar{c}_t \cdot \rho_p c_p} \tag{31}$$

Consequently, Eq. 28 and 29 may be expressed as

$$x_{max} = \frac{\rho_p L}{\rho_t} \ln \sqrt{\frac{\rho_t (v_o - v_c)^2}{2p_m}} + 1 \text{ and } \frac{x_{max}}{L} \approx \frac{\rho_p (v_o - v_c)^2}{2p_m} \qquad (32)$$

respectively.

Figure 6 is a plot of approximately 100 datum points derived from the normal impact of 0.25-inch-diameter-tool-steel cylinders of various lengths fired against 1 1/4-inch-thick targets of 2024-T4 aluminum. The data for this plot were taken from Ref. 20 and 21 and from personal communication from Backman. It may be noted that, below an initial velocity of 500 ft/sec, the data clearly define a straight line, in accordance with the second of Eq. 32. In this regime, the inertia term is small compared with the flow pressure, so that the approximation inherent in Eq. 29 is valid. Above this limit, the data tend to fall below the prediction of the approximation, which would be expected in a logarithmically dependent function. Consequently, Eq. 28 should apply in the domain above this velocity, where the inertial effects become appreciable. In any event, the plot appears to indicate that the mechanism of penetration suggested here, which requires a velocity-squared dependence, or, alternately, dependence upon the initial kinetic energy of the projectile, provides a superior fit of the data relative to the theory proposed by Backman, which indicates that penetration is more nearly a function of the initial projectile momentum.

There remains only the evaluation of the constant flow pressure and the value of the term v_c from the data and a comparison with predicted magnitudes on the basis of the theory of plasticity and Eq. 31. The values determined from Fig. 6 yield p_m = 225,000 psi and v_c = 63 ft/sec. The static yield stress of 2024-T4 aluminum is approximately 50,000 psi, and the corresponding dynamic value, using a 25% increase, is about 62,500 psi. Accordingly, the constant flow pressure should be $2.9\sigma_Y$, or 184,000 psi. The discrepancy between measured and predicted value is surprisingly small, especially when it is considered that the analysis neglected frictional effects which would raise the value of the predicted flow pressure considerably. The value of v_c computed from Eq. 31 is 66 ft/sec using the static value for σ_Y or 76 ft/sec with the dynamic value for σ_Y which may be considered to be excellent agreement with the measured value. The latter is quite difficult to determine from the graph and, furthermore, might yield a low value of v_c if the initial impact was even slightly removed from normal. Considering the approximations in the analysis, and the uncertainties of material behavior, agreement between theory and data is eminently satisfactory, particularly since the material constants can be predetermined by simply measuring the dynamic yield stress of the target.

Consider next the indentation into a semi-infinite target of an undeformable sphere of radius R and mass m, striking with initial velocity v_o, as shown in Fig. 7. For the range of impact velocities where total

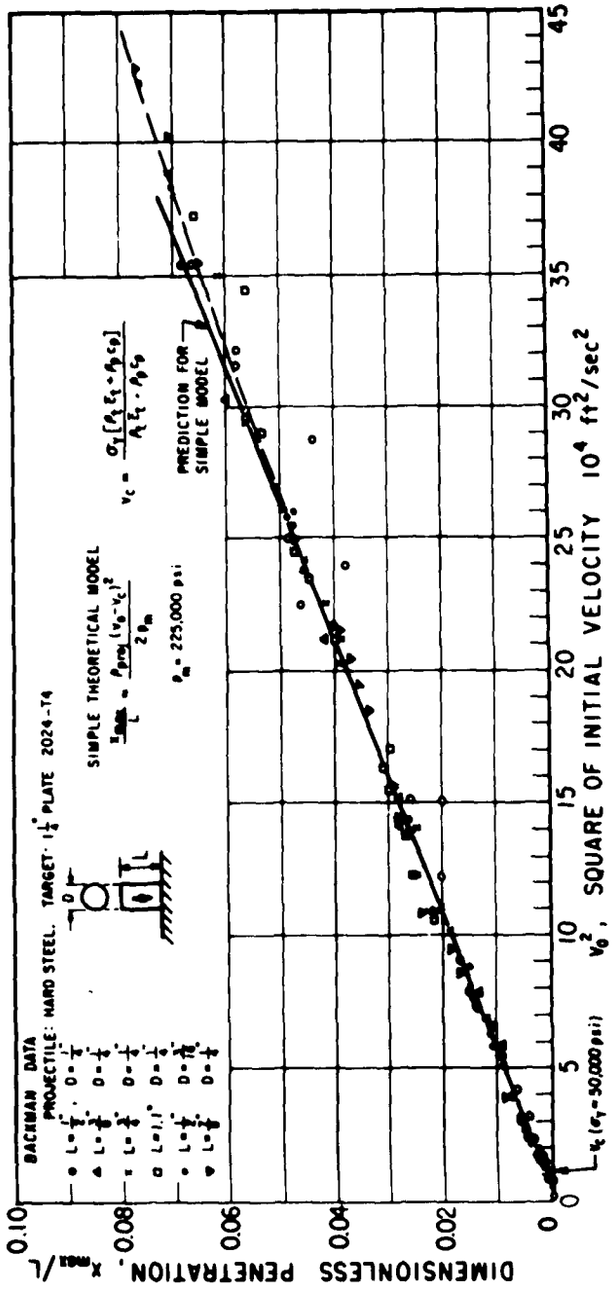

FIG. 6. Penetration Results for the Normal Impact of Steel Cylinders Against an Aluminum Target.

immersion does not occur, the equation of motion in the absence of friction is

$$-m\ddot{x} = \pi a^2 \left[p_m + \frac{1}{2}\rho_t \dot{x}^2\right] \tag{33}$$

where a is the radius of the indentation. From the relation

$$a^2 = 2Rx - x^2 \tag{34}$$

Eq. 33 may be written as

$$\ddot{x} + \frac{\pi\rho_t \dot{x}^2}{2m}(2Rx - x^2) + \frac{p_m}{m}\pi(2Rx - x^2) = 0 \tag{35}$$

Making the substitution $\frac{d^2x}{dt^2} \equiv \ddot{x} = -\dot{x}^3 \frac{d^2t}{dx^2} = -\dot{x}^3 t''$ in Eq. 35 yields[1]

$$t'' - \frac{1}{2}\frac{\pi\rho_t}{m} t'(2Rx - x^2) - \frac{p_m \pi}{m}(t')^3 (2Rx - x^2) = 0 \tag{36}$$

and further substitution of $z = \frac{1}{t'} = (\frac{dx}{dt})^2$ leads to the equation

$$\frac{dz}{dx} + -\frac{\pi\rho_t}{m} z\,(2Rx - x^2) + \frac{2p_m\pi}{m}(2Rx - x^2) = 0 \tag{37}$$

This is a standard linear differential equation whose integration is given by

$$z - z_o = v^2 - v_o^2 = -\left[\frac{2p_m\pi}{m} e^{-\frac{\pi\rho_t}{m}\int (2Rx-x^2)dx}\right] \int_o^x e^{\frac{\pi\rho_t}{m}\int (2Rx-x^2)dx} (2Rx-x^2)dx \tag{38}$$

$$= -\frac{2p_m}{\rho_t}\left[1 - e^{-\frac{\pi\rho_t}{m}(Rx^2 - \frac{x^3}{3})}\right]$$

From this equation, the maximum penetration x_{max} with $v = 0$ is determined from

$$1 - \frac{\rho_t v_o^2}{2p_m} = e^{-\frac{\pi\rho_t}{m}(Rx_{max}^2 - \frac{x_{max}^3}{3})} \tag{39}$$

which is obviously only valid for $\frac{\rho_t v_o^2}{2p_m} < 1$.

[1] Suggested by Dr. C. J. Thorne of the U. S. Naval Ordnance Test Station, China Lake, California.

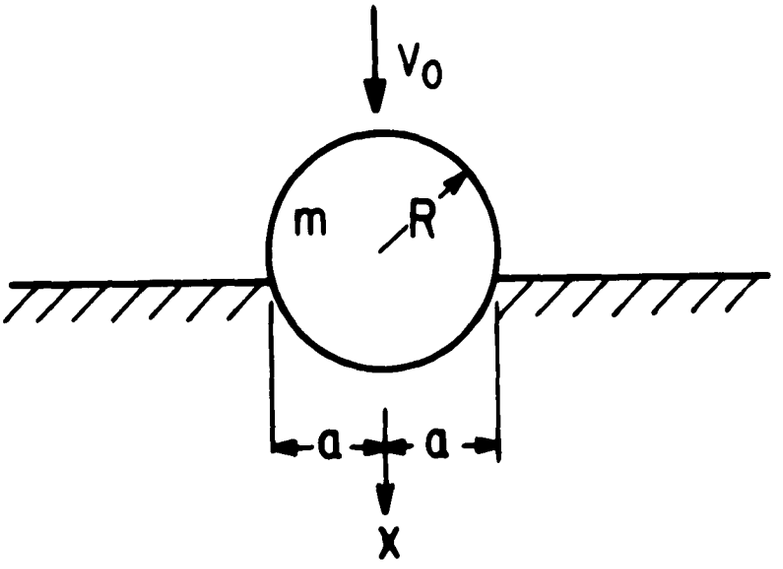

FIG. 7. Indentation Into a Semi-infinite Target of an Undeformable Sphere of Radius R and Mass m, Striking With Initial Velocity v_o.

For shallow immersion, $x^2 \ll 2Rx$, Eq. 39 reduces to

$$x_{max} = \sqrt{\frac{m}{\pi \rho_t R}} \ln \frac{2p_m}{2p_m - \rho_t v_o^2} \tag{40}$$

while for low velocities, when the inertial term can be neglected, Eq. 33 has the solution

$$v^2 - v_o^2 = -\frac{2\pi p_m}{m}\left[Rx^2 - \frac{x^3}{3}\right] \text{ or } v_o^2 = \frac{2\pi p_m}{m}\left[Rx_{max}^2 - \frac{x_{max}^3}{3}\right] \tag{41}$$

In the event that the last term on the right-hand side of Eq. 31 can also be neglected, corresponding to $x^2 \ll 2Rx$, the maximum penetration may be approximated by the relation

$$x_{max} = \sqrt{\frac{m}{2\pi R p_m}}\, v_o \tag{42}$$

It may be noted that the maximum penetration is here predicted to vary linearly with impact velocity, in contrast with the predictions for the cylindrical indenter as given by Eq. 32. Such approximately linear variation has been observed by a number of investigators for the partial

immersion of hard spheres into softer metals (Ref. 13 and 22). Figure 8 shows some experimental results from Ref. 13 regarding the penetration of a 0.50-inch-diameter hard steel sphere into the plane end of a 0.50-inch-diameter bar of 2024-T4 aluminum. According to this data, the mean flow pressure is calculated as $p_m = 325{,}000$. While this value is considerably at variance with that obtained from Fig. 6, the calculation is much more approximate, and both friction and lateral motion of the material, including the piling-up of the aluminum around the crater edge, have been neglected.

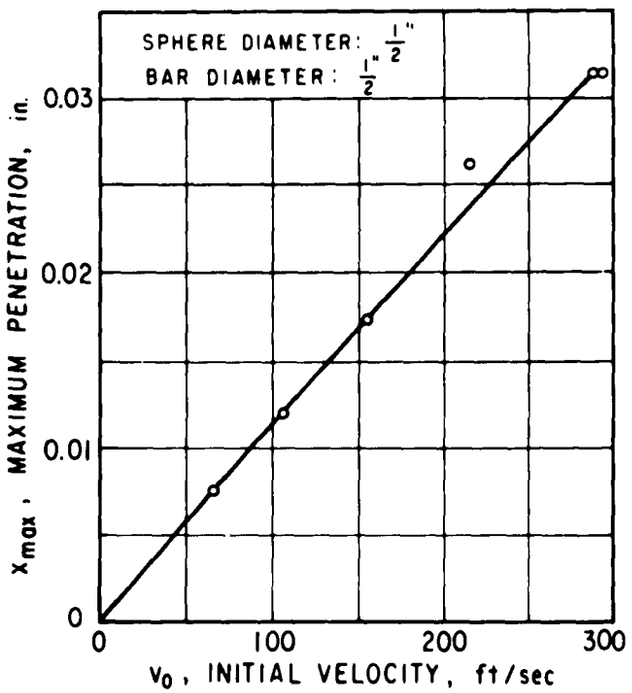

FIG. 8. Penetration of a Steel Sphere Into a 2024-T4 Aluminum Bar.

Once full immersion has occurred, Eq. 33 to 42 are no longer applicable. The analysis may then be carried out with the aid of Eq. 23 to 32, with the area term A replaced by πR^2, and $L\rho_p$ replaced by $m/\pi R^2$.

HYDRODYNAMIC THEORIES OF PENETRATION

The simplest hydrodynamic model of penetration assumes the existence of a continuous jet of a material of density ρ_j and constant jet velocity v_j penetrating a semi-infinite target of density ρ_t with penetration velocity U, also assumed constant. A pictorial representation for this model is shown in Fig. 9 for both a stationary and a moving frame of reference. For the assumed steady-state conditions, Bernoulli's equation at the stagnation point yields the expression (Ref. 9, 10, 14, and 15)

$$p_s = \frac{1}{2}\rho_t U^2 = \frac{1}{2}\rho_j (v_j - U)^2 \tag{43}$$

where p_s is interpreted as the stagnation pressure. Equation 43 assumes that the jet pressure is much greater than the yield strength σ_Y of the target; more generally, Eq. 43 may be expressed as (Ref. 17)

$$\frac{1}{2}\rho_t U^2 + k = \frac{1}{2}\rho_j (v_j - U)^2 \tag{44}$$

where, in the lower velocity region, k may be considered as the dynamic yield strength σ_{Y_D} of the material, and in the higher velocity regimes may also incorporate other dissipative effects such as compression and heating of the target, radiation of shock waves in the target, and energy losses due to impact explosions, when present. For a continuous jet of constant length L under the assumption that steady state is attained instantaneously, the penetration P can be expressed as

$$P = \int_0^{t_f} U dt = U t_f = UL/(v_j - U) \tag{45}$$

where t_f is the penetration time. For Eq. 43, the penetration may then be written as

$$P = L\sqrt{\frac{\rho_j}{\rho_t}} \tag{46}$$

while, for Eq. 44, this expression becomes

$$P = L\left[1 - \sqrt{\frac{\rho_t}{\rho_j} + \frac{2k}{\rho_j v_j^2}\left(1 - \frac{\rho_t}{\rho_j}\right)}\right] \Bigg/ \left[\sqrt{\frac{\rho_t}{\rho_j} + \frac{2k}{\rho_j v_j^2}\left(1 - \frac{\rho_t}{\rho_j}\right)} - \frac{\rho_t}{\rho_j}\right] \tag{47}$$

Alternatively, an equation accounting for the yield strength of the target has been proposed in the form (Ref. 18)

$$P = L\sqrt{\frac{\rho_j}{\rho_t}}\left(1 - q\,\frac{\sigma_{Y_D}}{\rho_j v_j^2}\right) \tag{48}$$

where q is a function of ρ_j and ρ_t; estimates indicate that the terms $q(\sigma_{Y_D}/\rho_j v_j 2)$ may attain a value as high as 0.3 for armor plate subjected to shaped charge action, but is negligible for a lead target.

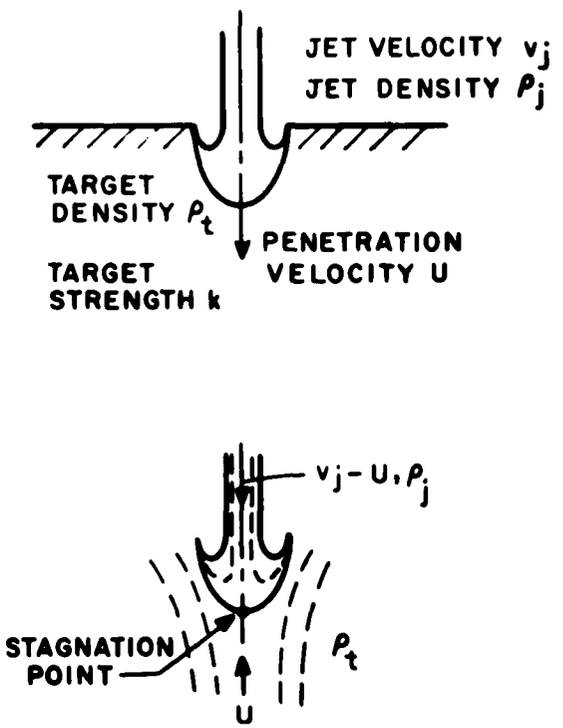

FIG. 9. Hydrodynamic Model of Penetration for Both a Stationary and a Moving Frame of Reference.

For a jet consisting of particles rather than a continuous stream, it may be assumed that inelastic impacts are produced against the target surface. The pressure exerted by the jet, considered as the change of momentum divided by the jet area, A, is then given by

$$p = \rho_j A(v_j - U)^2/A = \frac{1}{2}\rho_t U^2 \qquad (49)$$

and Eq. 46 becomes

$$P = L\sqrt{\frac{2\rho_j}{\rho_t}} \tag{50}$$

It may thus be concluded (Ref. 14) that for any jet striking a target, the expression for the penetration in the simple model described above can be written as

$$P = L\sqrt{\frac{\lambda\rho_j}{\rho_t}} \quad \text{where} \quad 1 \leq \lambda \leq 2 \tag{51}$$

when the strength of the target is neglected. Experimental verification of the validity of Eq. 51 (Ref. 19) did not, however, provide any indication that the parameter λ ever significantly exceeded a value of unity. The possibility was suggested that the actual jet did not fracture into sufficiently small enough components so that the mechanism described by Eq. 49 was a valid description of the process. For single pellets of comparable size, on the other hand, the inelastic impact process stipulated by this relation has been substantiated by observation.

The simple model described above is not always satisfactory in comparison with experiments. At very high jet velocities, the target strength can be neglected, but other dissipative effects must be considered in terms of the quantity k; at low jet velocities, the dynamic strength of the target can not be disregarded. Furthermore, Eq. 46, 47, 48, 50, and 51 do not indicate any dependence of the penetration upon standoff, whereas experimental results (Ref. 18) show a variation with this parameter; the effect of standoff is primarily the creation of a velocity gradient in the jet which bears upon the fundamental steady-state assumption in the derivation of the relations. It has been shown that, for a linear velocity gradient, the formulas given above can be applied to most metals at a given standoff, provided the latter is not too small (Ref. 18).

In addition to the considerations cited above, there will exist a further expansion of the target material beyond the instant of termination of jet action due to the presence of a dynamic flow pressure causing flow of the target. This additional penetration, called residual or secondary penetration, is concluded only when this pressure has been reduced to the value of σ_{Y_D}. One version of this secondary penetration P_2, based upon the model shown in Fig. 9, an assumed hemispherical expansion during residual penetration and a uniform pressure distribution at the contact surface during primary penetration (Ref. 18), simply equates P_2 to the radius of the hole produced by the jet. When the jet is considered as a rod penetrating a half-space, the plastically deformed hole in the target is essentially cylindrical (Ref. 17), and for large values of L/A and P/A, the final crater volume V_f can be expressed as

$$V_f = \int_o^P \int_A^{A_f} kdAdP/(\tfrac{1}{2}\rho_t U^2) \qquad (52)$$

where A_f is the final cross-sectional area of the hole. Upon substitution from Eq. 44 and 47 in Eq. 52, it may also be shown that the final crater volume can be written as

$$V_f = \tfrac{1}{2} LA\rho_j v_j^2/4\bar{k} \equiv T_o/4\bar{k} \qquad (53)$$

where $\bar{k}$ is the average dynamic yield strength during the secondary penetration process and T_o is the kinetic energy of the jet just before striking the target. The threshhold of jet velocity just producing plastic deformation of the target, v_T, may be approximated from Eq. 53 by assuming no flow and equating V_f to the projectile volume LA, so that

$$v_T \approx \sqrt{\frac{8\sigma_Y}{\rho_j}} \qquad (54)$$

Presumably, the models considered above are valid in a region of jet velocity v_j ranging from v_T to v_c, where v_c is the critical velocity beyond which impact explosions may be expected.

Observed values of the ratio U/v_j as a function of v_j from tests involving the penetration of shaped charges with steel liners into steel, aluminum, and lead targets (Ref. 17 and 19) have been compared with the predictions of Eq. 43 in the form

$$U/v_j = \frac{1}{\sqrt{\rho_t/\rho_j} + 1} = \text{constant for a particular set of materials} \qquad (55)$$

The variation in jet velocity was obtained by increasing the standoff of the charge. It was found that Eq. 55 provides a surprisingly good approximation with the experimental data in the range $4v_T < v_j < v_c$, but indicated a considerable deviation in the regime $v_T < v_j < 4v_T$. Use of Eq. 44 with an evaluation of the term k by theoretical considerations provided a much better correlation in this lower velocity regime (Ref. 17). Comparison of test results of the final crater volume with Eq. 53, using the static yield strength of $\bar{k}$, proved to be inconclusive.

The work of compression per unit volume on the target may be determined from the relation

$$k_p = -\int_1^{\rho/\rho_o} pdV/V \qquad (56)$$

which may be evaluated in conjunction with any of the equations of state of the target material suggested in the literature, such as that given in Ref. 17 or the Pack, Evans, and James relation (Ref. 23)

$$p = \frac{B_1}{(\rho_o/\rho)^{2/3}} \left[e^{B_2 \left\{ 1 - \left(\frac{\rho_o}{\rho}\right)^{1/3} \right\}} - 1 \right] \tag{57}$$

(with pressures in megabars and densities in g/cm^3), where constants B_1 and B_2 for some metals are given in Table 1 (Ref. 24).

TABLE 1. Constants for Eq. 57 for Several Metals as Determined From Hydrostatic Compressibility Measurements

Material	B_1, Megabars	B_2	ρ_{o_t}, g/cm^3
Aluminum...	0.2209	9.802	2.699
Copper.....	0.3810	10.829	8.88
Iron.....	0.624	8.099	7.88
Lead.....	0.1002	12.379	11.34
Magnesium..	0.3996	3.115	1.741
Uranium....	0.1172	25.008	18.70

It should be noted that the pressure level determining the contribution of the work of compression as well as that for shock heating should be taken as the flow pressure of the target, $1/2\ \rho_t U^2$. The energy due to shock heating, representing the difference between shock and adiabatic compression $T(S_c - S_a)$, where T is temperature and S is entropy, has been shown to be approximately given on a unit volume basis by the relation (Ref. 24)

$$k_h \approx \bar{c}_s\ Z\ \left(\frac{\rho}{\rho_o} - 1\right)^3 / \left(\frac{\rho}{\rho_o}\right)^3 \tag{58}$$

Here k_h is the pressure associated with this phenomenon, $\bar{c}_s$ is the average heat capacity per unit volume, and Z is a constant computed as $1.88 \cdot 10^4$, $1.53 \cdot 10^4$, $1.84 \cdot 10^4$, and $1.26 \cdot 10^4$ °K for iron, lead, copper, and aluminum, respectively (Ref. 17). The value of k is thus given by

$$k = k_p + k_h + \sigma_{Y_D} \tag{59}$$

when the energy associated with shock wave radiation is neglected. A good analytical description for this component has not as yet been devised.

It has been suggested (Ref. 16) that the threshhold for impact explosion will be reached when the work of compression and shock heating reaches a critical level defined by

$$(k_p + k_h)_c = \rho_t E_c / N \tag{60}$$

where E_c is the molar cohesive energy and N the atomic weight of the material. In Eq. 60, other contributions to the quantity k have been neglected on an order of magnitude basis. The total volume of the crater generated under these conditions consists of two zones: (1) a region of the target where vaporization occurs, denoted by V_a, and (2) the region of secondary plastic deformation V_b. In the first zone, it may be assumed that the conditions are the same as if an explosive having the same available energy T_a were detonated in the same volume V_a. The energy is then given by

$$T_a = \frac{1}{2} m v_j^2 - V_a (k_p + k_h)_c = \frac{1}{2} V_a \rho_t U_c^2 \tag{61}$$

from which

$$V_a = \frac{1}{2} m v_j^2 / (\{k_p + k_h\}_c + \frac{1}{2} \rho_t U_c^2) = \frac{1}{2} m v_j^2 / p_c \tag{62}$$

where m is the total projectile mass and $1/2\ mv_j^2$ is its kinetic energy before impact. The crater developed during the second zone is again described by Eq. 53, so that the total volume for this type of impact can be represented by

$$V = V_a + V_b = V_a (1 + \rho_t U_c^2 / 8\bar{k}) \tag{63}$$

Since $\rho_t U_c^2 \gg 8\bar{k}$, the crater produced by vaporization of the target material is very small compared to that produced by residual plastic deformation.

ÖPIK'S THEORY OF CRATERING[2]

A theory of penetration of meteorites has been developed based upon a model considering both the meteorite and the target as incompressible fluids. For convenience, the striker is assumed to consist of a cylinder

[2]References 9 and 10.

of radius r_o, height $h_o = 2r_o$, and mass $m = 2\pi\rho_m r_o^3$, with ρ_m as the meteorite density. In actual practice, the exact shape of the meteorite should not exert a deciding influence on the phenomenon. The penetration process is assumed to be that shown in Fig. 10, with the striker flattening at right angles to the direction of motion, while the target strength is characterized by a pressure p_D representing the resistance to plastic flow or fracture; this parameter is entirely analogous to the dynamic flow pressure assumed in previous models. If, now, r and h represent the dimensions of the striker during penetration, conservation of mass yields

$$r^2 h = 2r_o^3 \tag{64}$$

Denoting the surface coordinate of the meteor in contact with the target by z and the coordinate of the mass center of the meteor by $\bar{z}$, then

$$\dot{h} = 2(\dot{z} - \dot{\bar{z}}) \qquad \text{and from Eq. 64} \qquad \dot{r} = \tfrac{1}{2}(r/r_o)^3(\dot{\bar{z}} - \dot{z}) \tag{65}$$

The equation of motion for the meteorite, striking with initial velocity v_o, is

$$m\ddot{\bar{z}} = -\pi r^2 p \tag{66}$$

where p, the penetration resistance, is assumed to be given by the relation

$$p = \tfrac{1}{2}\rho_t \dot{z}^2 + p_D \tag{67}$$

and the resistance to radial expansion, p', is hypothesized as

$$p' = \tfrac{1}{2}\rho_t \dot{r}^2 + p_D \tag{68}$$

It is now assumed artificially that

$$p = p' + \tfrac{1}{2}\rho_m \dot{r}^2 \tag{69}$$

This corresponds to a Bernoulli equation for irrotational flow in a reference frame moving with velocity $\dot{z}$. Here p, the Bernoulli constant, would be the stagnation pressure; but, of course, the flow is not actually steady.

Equations 64–69, together with initial conditions $r = r_o$, $z = 0$, $\dot{\bar{z}} = v_o$, can be integrated numerically, as detailed in Ref. 9 and 10. The volume of the crater generated can also be deduced as a rough estimate. It may be observed that, in spite of the relatively crude assumptions underlying the present analysis, there exists good agreement between the predictions concerning the crater volume and measurements of crater dimensions for steel jets penetrating steel targets (Ref. 10).

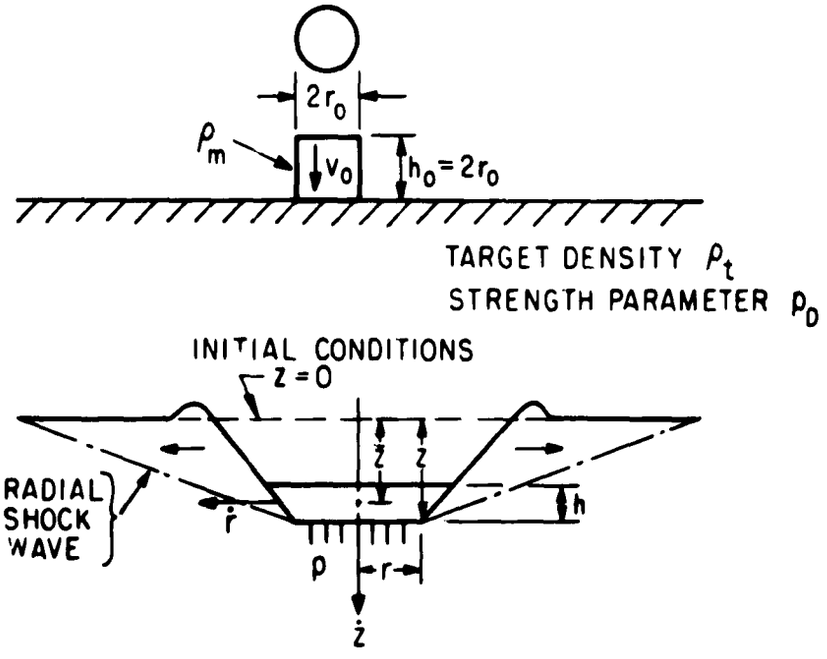

FLOW PATTERN DURING PENETRATION

FIG. 10. Flow Pattern During Penetration. Assumed penetration process for meteoritic impact.

REFERENCES

1. Love, A. E. H. A Treatise on the Mathematical Theory of Elasticity. New York, Dover, 1944.

2. Timoshenko, S. P., and J. N. Goodier. Theory of Elasticity, 2nd ed. New York, McGraw-Hill, 1951.

3. Whiffin, A. C. "The Use of Flat-ended Projectiles for Determining Dynamic Yield Stress. Part II. Tests on Various Metallic Materials," ROY SOC LONDON, PROC, A, Vol. 194 (1948), p. 300.

4. Campbell, J. D. "The Yield of Mild Steel Under Impact Loading," J MECH PHYS SOLIDS, Vol. 3 (1954), p. 54.

5. Goldsmith, W. Impact. London, Edward Arnold, 1960.

6. Hertz, H. "Über die Berührung fester elastischer Körper," J REINE ANG MATH (CRELLE), Vol. 92 (1881), p. 155.

7. Davies, R. M. "The Determination of Static and Dynamic Yield Stresses Using a Steel Ball," ROY SOC LONDON, PROC, A, Vol. 197 (1949), p. 416.

8. Hill, R. The Mathematical Theory of Plasticity. Oxford Univ. Press, 1950.

9. Öpik, E. "Researches on the Physical Theory of Meteor Phenomena: Part I. Theory of the Formation of Meteor Craters," ACTA ET COMM UNIV TARTUENSIS, 1936.

10. Rostoker, N. "The Formation of Craters by High-speed Particles," METEORITICS, Vol. 1, No. 1 (1953), p. 11.

11. Tabor, D. The Hardness of Metals. Oxford, Clarendon Press, 1951.

12. Crook, A. W. "A Study of Some Impacts Between Metal Bodies by a Piezoelectric Method," ROY SOC LONDON, PROC, A, Vol. 212 (1952), p. 377.

13. Goldsmith, W., and P. T. Lyman. "The Penetration of Hard Steel Spheres into Plane Metal Surfaces," J APP MECH, Vol. 27 (1960), p. 717.

14. Pugh, E. M., R. J. Eichelberger, and N. Rostoker. "Theory of Jet Formation by Charges with Lined Conical Cavities," J APPL PHYS, Vol. 23 (1952), pp. 532, 537.

15. Birkhoff, C., D. P. MacDougall, E. M. Pugh, and G. Taylor. "Explosives with Lined Cavities," J APPL PHYS, Vol. 19 (1948), p. 563.

16. Cook, M. A. The Science of High Explosives. New York, Reinhold, 1958.

17. ------. "Mechanism of Cratering in High-Velocity Impact," J APPL PHYS, Vol. 20 (1959), p. 725.

18. Pack, D. C., and W. M. Evans. "Penetration by High Velocity Jets," PHYS SOC LONDON, PROC, V., Vol. 64, p. 298.

19. Eichelberger, R. J. "Experimental Test of the Theory of Penetration by Metallic Jets," J APPL PHYS, Vol. 27 (1956), p. 63.

20. U. S. Naval Ordnance Test Station. Elastic and Plastic Behavior in Simple Target-Projectile Systems, by Marvin E. Backman. China Lake, Calif., NOTS, 4 November 1957. (NAVORD Report 5593, NOTS 1798).

21. Backman, M. E. "Elastic and Plastic Behavior in the Impact of Cylinders Against Plates," J APPL PHYS, Vol. 30 (1959), p. 1397.

22. Engel, O. G. "Pits in Metals Caused by Collision with Liquid Drops and Soft Metal Spheres," NATL BUR STANDARDS, J RES, Vol. 62 (1959), p. 229.

23. Pack, D. C., W. M. Evans, and H. J. James. "The Propagation of Shock Waves in Steel and Lead," PHYS SOC LONDON, PROC, Vol. 60 (1948), p. 1.

24. Duvall, G. E., and B. J. Zwolinski. "Entropic Equations of State and Their Application to Shock Wave Phenomena in Solids," ACOUS SOC AM, J, Vol. 27 (1955), p. 1054.

INITIAL DISTRIBUTION

18 Chief, Bureau of Naval Weapons
- R-363 (1)
- RAAV (1)
- RAAV-34 (1)
- RM-3 (1)
- RMMO-4 (2)
- RMMO-5 (1)
- RMMO-512 (1)
- RMMO-522 (1)
- RR (1)
- RRRE (1)
- RRRE-5 (1)
- RSSH-32 (1)
- RU (1)
- RUME-11 (1)
- RUME-3 (2)
- RUTO-2 (1)

5 Chief of Naval Operations
- Deputy Chief for Air (1)
- Operations Evaluation Group (2)
- OP-55 (1)
- OP-721D (1)

3 Chief of Naval Research
- Code 104 (1)
- Code 429 (1)
- Code 461 (1)

1 Air Development Squadron 5, Naval Air Facility, China Lake
1 David W. Taylor Model Basin
1 Fleet Anti-Air Warfare Training Center, San Diego
1 Naval Air Force, Atlantic Fleet
2 Naval Air Force, Pacific Fleet
1 Naval Air Material Center, Philadelphia
2 Naval Air Mobile Training, Naval Air Station, Miramar
- Naval Air Mobile Training Detachment, 4003 Ordnance (1)
- Naval Air Mobile Training Detachment, 4030 Missile (1)

1 Naval Air Station, North Island
2 Naval Air Test Center, Patuxent River (Aeronautical Publications Library)
1 Naval Avionics Facility, Indianapolis (Library)
1 Naval Missile Center, Point Mugu (Technical Library)
1 Naval Ordnance Laboratory, White Oak (Guided Missile Warhead Section)
1 Naval Postgraduate School, Monterey

2 Naval Propellant Plant, Indian Head (Research and Development Department)
1 Naval Research Laboratory (Chemistry Division, Code 6130, R. R. Miller)
1 Naval Weapons Laboratory, Dahlgren (Technical Library)
2 Naval Weapons Services Office, Naval Weapons Plant
1 Office of Naval Research Branch Office, Chicago
1 Office of Naval Research Branch Office, Pasadena
1 Operational Test and Evaluation Force
1 Bureau of Naval Weapons Representative, Azusa
2 Chief of Ordnance
    ORDTB (1)
    ORDTS (1)
2 Aberdeen Proving Ground
    Ballistic Research Laboratories (1)
    Development and Proof Services (1)
1 Army Research Office, Durham
1 Diamond Ordnance Fuze Laboratory (Library)
4 Frankford Arsenal
    Pitman-Dunn Laboratory (3)
    Library (1)
1 Ordnance Ammunition Command, Joliet (ORDLY-R-T)
1 Ordnance Test Activity, Yuma Test Station (A and A Division, S. Cohen)
3 Picatinny Arsenal (Library)
1 Radford Arsenal
1 Redstone Arsenal (Rocket Development Laboratory, Test and Evaluation Branch)
1 Rock Island Arsenal
3 White Sands Proving Ground (Technical Library)
2 Headquarters, U. S. Air Force
    AFDRD-AN (1)
    AFDRD-CC (1)
1 Air Force Cambridge Research Laboratories, Laurence G. Hanscom Field
3 Air Proving Ground Center, Eglin Air Force Base
1 Air Research and Development Command, Andrews Air Force Base
1 Air University Library, Maxwell Air Force Base
1 Holloman Air Force Base
1 Tactical Air Command, Langley Air Force Base (TPL-RQD-M)
1 AFSC Liaison Office, Aberdeen Proving Ground
1 Defense Atomic Support Agency, Sandia Base
1 Weapons Systems Evaluation Group
1 Ames Research Center
1 Langley Research Center (Library)
1 Lewis Research Center
4 British Joint Services Mission, Ministry of Supply Staff (Reports Officer) via BuWeps (DSC)
4 Defence Research Member, Canadian Joint Staff (W) via BuWeps (DSC)
2 Aerojet-General Corporation, Azusa, Calif. (Librarian) via BuWepsRep
2 Allegany Ballistics Laboratory, Cumberland, Md.
2 Applied Physics Laboratory, JHU, Silver Spring
1 Armour Research Foundation, Chicago (Document Librarian for Department M)

ABSTRACT CARD

U. S. Naval Ordnance Test Station
Analytical Versions of Penetration Processes, by Werner Goldsmith. China Lake, Calif., NOTS, February 1962. 34 pp. (NAVWEPS Report 7812, NOTS TP 2811), UNCLASSIFIED.
Distribution includes GM List No. 23, MML 200/23, 3 April 1961, Parts A and DW.

(Over)
2 cards, 4 copies

U. S. Naval Ordnance Test Station
Analytical Versions of Penetration Processes, by Werner Goldsmith. China Lake, Calif., NOTS, February 1962. 34 pp. (NAVWEPS Report 7812, NOTS TP 2811), UNCLASSIFIED.
Distribution includes GM List No. 23, MML 200/23, 3 April 1961, Parts A and DW.

(Over)
2 cards, 4 copies

U. S. Naval Ordnance Test Station
Analytical Versions of Penetration Processes, by Werner Goldsmith. China Lake, Calif., NOTS, February 1962. 34 pp. (NAVWEPS Report 7812, NOTS TP 2811), UNCLASSIFIED.
Distribution includes GM List No. 23, MML 200/23, 3 April 1961, Parts A and DW.

(Over)
2 cards, 4 copies

U. S. Naval Ordnance Test Station
Analytical Versions of Penetration Processes, by Werner Goldsmith. China Lake, Calif., NOTS, February 1962. 34 pp. (NAVWEPS Report 7812, NOTS TP 2811), UNCLASSIFIED.
Distribution includes GM List No. 23, MML 200/23, 3 April 1961, Parts A and DW.

(Over)
2 cards, 4 copies

NAVWEPS REPORT 7812

ABSTRACT. In the interest of obtaining a comprehensive view of the penetration of bodies into solid plates some of the more prominent theoretical relations used to describe penetration processes are outlined and correlated. The velocity ranges to which these relations apply and the assumptions used in the analytical developments are summarized. Elastic behavior processes in impact are first discussed in order to establish lower bounds on the impact velocity for the formation of a crater. Various analytical representations of crater formation

(Contd. on Card 2)

NAVWEPS Report 7812

ABSTRACT. In the interest of obtaining a comprehensive view of the penetration of bodies into solid plates some of the more prominent theoretical relations used to describe penetration processes are outlined and correlated. The velocity ranges to which these relations apply and the assumptions used in the analytical developments are summarized. Elastic behavior processes in impact are first discussed in order to establish lower bounds on the impact velocity for the formation of a crater. Various analytical representations of crater formation

(Contd. on Card 2)

NAVWEPS Report 7812

ABSTRACT. In the interest of obtaining a comprehensive view of the penetration of bodies into solid plates some of the more prominent theoretical relations used to describe penetration processes are outlined and correlated. The velocity ranges to which these relations apply and the assumptions used in the analytical developments are summarized. Elastic behavior processes in impact are first discussed in order to establish lower bounds on the impact velocity for the formation of a crater. Various analytical representations of crater formation

(Contd. on Card 2)

NAVWEPS Report 7812

ABSTRACT. In the interest of obtaining a comprehensive view of the penetration of bodies into solid plates some of the more prominent theoretical relations used to describe penetration processes are outlined and correlated. The velocity ranges to which these relations apply and the assumptions used in the analytical developments are summarized. Elastic behavior processes in impact are first discussed in order to establish lower bounds on the impact velocity for the formation of a crater. Various analytical representations of crater formation

(Contd. on Card 2)

ABSTRACT CARD

U. S. Naval Ordnance Test Station
Analytical Versions of . . . (Card 2)
processes are summarized and the advantages of the theory of constant dynamic flow pressure are demonstrated by calculated results which agree well with experimental penetration data from several sources. The hydrodynamic theory of penetration and Öpik's theory of penetration are discussed in relation to these conclusions on crater formation.

NAVWEPS Report 7812

U. S. Naval Ordnance Test Station
Analytical Versions of . . . (Card 2)
processes are summarized and the advantages of the theory of constant dynamic flow pressure are demonstrated by calculated results which agree well with experimental penetration data from several sources. The hydrodynamic theory of penetration and Öpik's theory of penetration are discussed in relation to these conclusions on crater formation.

NAVWEPS Report 7812

U. S. Naval Ordnance Test Station
Analytical Versions of . . . (Card 2)
processes are summarized and the advantages of the theory of constant dynamic flow pressure are demonstrated by calculated results which agree well with experimental penetration data from several sources. The hydrodynamic theory of penetration and Öpik's theory of penetration are discussed in relation to these conclusions on crater formation.

NAVWEPS Report 7812

U. S. Naval Ordnance Test Station
Analytical Versions of . . . (Card 2)
processes are summarized and the advantages of the theory of constant dynamic flow pressure are demonstrated by calculated results which agree well with experimental penetration data from several sources. The hydrodynamic theory of penetration and Öpik's theory of penetration are discussed in relation to these conclusions on crater formation.

NAVWEPS Report 7812